



Measurements of NaCl in Ambient Air with a Capture Vaporizer-ToF-ACSM

Marije van den Born¹, Hengjia J. Ou², Jan Mulder¹, Jinglan Fu^{1,3}, Harald Saathof³, Ulrike

5 Dusek¹

¹Centre for Isotope Research (CIO), Energy and Sustainability Research Institute Groningen (ESRIG),
University of Groningen, Groningen, 9747 AG, the Netherlands

²Guangzhou Institute of Tropical and Marine Meteorology, China Meteorological Administration, Guangzhou
510640, China

10 ³Institute of Meteorology and Climate Research – Atmospheric Aerosol Research, Karlsruhe Institute of
Technology, Karlsruhe, Germany

Correspondence to: Marije van den Born (marije.van.den.born@rug.nl)

CONTACT M. van den Born marije.van.den.born@rug.nl Centre for Isotope Research (CIO), Energy and Sustainability

Research Institute Groningen (ESRIG), University of Groningen, Nijenborgh 6, Energy Academy Europe, Groningen, Gr.,

15 9747 AG, the Netherlands

Abstract. Sea spray aerosol is important for climate and atmospheric chemistry by influencing radiative forcing and heterogeneous reactions, but few online methods exist for quantifying sub-micron sea spray concentrations. Common chemical speciation instruments, such as aerosol mass spectrometers (AMS) and aerosol chemical speciation monitors (ACSM), are usually not used for sea salt quantification due to the incomplete evaporation of refractory sodium chloride (NaCl). This study evaluates the capability of the time-of-flight-ACSM (ToF-ACSM) equipped with a capture vaporizer (CV) to detect and quantify sea salt aerosol for the first time. Key NaCl marker ions (m/z 23 (Na), m/z 58 (Na^{35}Cl) and m/z 60 (Na^{37}Cl) were identified through a controlled laboratory calibration. The calibration experiments show that when the ACSM response (ions/s) is normalized by the available particle surface area, the response is independent of particle concentration and only weakly dependent on particle size for monodisperse NaCl aerosol. When considering aerosol mass concentrations without normalization for the available particle surface area, it is only possible to derive ambient sea salt mass concentrations from the ACSM signal with prior information on particle size due to the observed size dependence. Furthermore, controlled chamber experiments indicated that secondary organic aerosol (SOA) formed from α -pinene as a precursor and condensed on the NaCl particles does not produce significant amounts of fragments at the m/z values characteristic for NaCl. Field experiments at a coastal site showed that conditions with onshore winds resulted in high correlations ($R^2 = 0.949\text{--}0.977$) between the three key NaCl marker ions. By applying the laboratory-derived calibration formula to the raw CV-ToF-ACSM m/z 23 signal, sea-salt aerosol surface concentrations could be quantitatively determined in real time. However, the slope between the fragments at m/z 23 and m/z 58 is lower in the ambient data than in the laboratory calibration, suggesting reduced Cl relative to Na due to aging reactions of the sea salt particles in the coastal environment. Overall, these results demonstrate that the CV-ToF-ACSM can provide quantitative real-time information on submicron sea salt aerosol before ageing, particularly in terms of surface area, while accurate mass concentration retrieval requires additional NaCl size



distribution information. These findings highlight the potential to improve the characterization of marine aerosol sources and their role in atmospheric processes.

40 **1 Introduction**

Atmospheric aerosols interact in particular with solar radiation and clouds, altering the Earth's radiation balance and therefore contribute to climate change. Uncertainties related to aerosol-cloud interactions and their effects on radiative forcing represent a primary source of variability in anthropogenic forcing estimates (Lee et al., 2016). Reducing these uncertainties necessitates reliable measurements of the spatial, physical, and chemical properties of aerosols (Bellouin et al., 2020).

Among the different aerosol types, sea salt particles, primarily composed of sodium chloride (NaCl), play a major role in the Earth's radiative balance and cloud microphysics due to their high hygroscopicity and ability to act as cloud condensation nuclei (CCN). They are a dominant component of natural aerosol mass, particularly in marine and coastal environments, and significantly influence both direct and indirect radiative forcing (O'Dowd et al., 2002). Because of their ionic nature and relatively large particle sizes, sea salt aerosols (SSA) are most commonly quantified using filter-based sampling methods, followed by ion chromatographic analysis of water-soluble inorganic species. However, while filter-based approaches offer reliable bulk composition data, they lack the temporal resolution needed to capture rapid variations in aerosol composition.

This study utilizes a time-of-flight aerosol chemical speciation monitor (ToF-ACSM), an instrument designed for routine measurement of the mass and chemical composition of non-refractory (NR) aerosol components (Fröhlich et al., 2013). ACSM instruments typically use a standard vaporizer (SV). To diminish the effects of particle bounce, the capture vaporizer (CV) was developed (Xu et al., 2018). The CV contains an inner cavity to reduce the effects of particle bounce, therefore improving the collection efficiency (CE) of the instrument to ~ 1 . Although the CV improves CE compared to the SV, its structure increases aerosol particle residence time, which can alter thermal decomposition and result in distinct fragmentation patterns, also due to the different operation temperature of the CV (~ 550 °C) (Zheng et al., 2020).

Sea salt is not routinely measured in ACSMs, because it does not fully vaporize due to its refractory nature and vaporization temperature requirements ($> \sim 600$ °C) (Bahreini et al., 2003; Zhang et al., 2011). Nevertheless, partial evaporation of ambient sea salt at temperatures of ~ 600 °C had been demonstrated earlier (O'Dowd and Smith, 1993).

At coastal measurement sites, NaCl fragments from sea salt aerosols have been detected both by the aerosol mass spectrometer (AMS) and ACSM instruments using the SV. Various studies (Mallet et al., 2016; Nuaaman et al., 2015; Ovadnevaite et al., 2012; Schmale et al., 2013) have attempted to quantify sea salt mass concentrations using AMS with mixed results, but, to our knowledge, this has not been reported previously for CV-ToF-ACSM instruments.

Freney et al. (2021) reported typical signature peaks for SSA (m/z fragments at m/z 23 (Na^+), m/z 35 and 37 ($^{35}\text{Cl}^-$, $^{37}\text{Cl}^-$), 58 and 60 (Na^{35}Cl , Na^{37}Cl), and 81 and 83 (NaCl^2 , $\text{NaCl}^{37}\text{Cl}$)) during shipboard measurements while SSA was generated using a bubble-bursting apparatus. The NaCl signals were confirmed through controlled experiments with pure NaCl aerosol particles. In another previous study an in-situ particle generator was utilized aboard a ship to produce sea spray particles, which were measured by a quadrupole-AMS (Q-AMS) and a high-resolution ToF-AMS (HR-ToF-AMS), both detecting NaCl fragments (Na^{35}Cl and Na^{37}Cl) at the samples which had elevated SSA



75 concentrations (Bates et al., 2012). In another study, Timonen et al. (2016) observed NaCl signature peaks (m/z 58
and 60) in SV-ToF-ACSM mass spectra at the Neumayer Station, Antarctica, under sea salt aerosol influence as
indicated by air mass back trajectory analysis. The peaks at m/z 58 and 60 were measured together with high chloride
signals, and when neither methanesulfonic acid (MSA) or organic aerosol was elevated. In a recent study, the
interference of SSA with biomass burning organic aerosol (BBOA) measurements was examined, given that BBOA
80 is typically characterized by ion markers at m/z 60 and m/z 73, representing $C_2H_4O_2^+$ and $C_3H_5O_2^+$ ions respectively.
The presence of $Na^{37}Cl^+$ ions, which also have a mass-to-charge ratio of 60, can interfere with the BBOA marker at
 m/z 60 when using the CV. In that study, a CV-ToF-ACSM was deployed at two coastal sites in Australia, where
distinct correlations were observed between the ion signal at m/z 60 and the secondary BBOA marker at m/z 73.
Positive Matrix Factorization (PMF) analysis further confirmed that the signal at m/z 60 could originate from both
85 NaCl in sea salt and BBOA (Sutresna et al., 2024).
Quantification of SSA mass concentrations was previously attempted by Ovadnevaite et al. (2012), who used a HR-
ToF-AMS to measure sea salt concentrations as a function of wind speed at the Mace Head Atmospheric Research
Station in Ireland. Utilizing $Na^{35}Cl$ as a proxy for SSA, they established a calibration scaling factor of 51 between
AMS-reported NaCl loadings and actual sea salt present in PM_{10} . This calibration was derived from comparisons with
90 synthetic SSA standards and with a vaporizer temperature of $\sim 650^\circ$. Schmale et al. (2013) subsequently applied this
scaling factor to estimate SSA mass contributions based on HR-ToF-AMS data. Petters et al. (2023) also incorporated
this scaling factor in their study of nano plastics within sea spray aerosol. Additionally, Zorn et al. (2008) reported a
chloride-to-sea salt scaling factor between 150 and 220, based on comparisons between AMS and particle-into-liquid
sampler measurements.
95 In this study, we evaluate the potential for quantifying NaCl using a CV-ToF-ACSM in a coastal environment. We
investigate the most suitable marker ions for NaCl quantification, exploring the use of characteristic m/z signal ratios
to confirm the presence of NaCl in ambient data. A laboratory calibration is employed to derive NaCl concentrations
from measured mass fragments. In addition, chamber experiments conducted at the AIDA facility (Saathoff et al.,
2009; Wagner et al., 2021) in 2024 investigate the formation of secondary organic aerosol (SOA) from α -pinene on
100 NaCl seed particles in order to assess potential interferences of typical SOA fragments with the ACSM-based detection
of NaCl. Finally, we also use long term ACSM data recorded at a coastal site in the Netherlands and a more inland
site in the Netherlands to study the applicability and the limits of the method that was developed.

2 Methods

105 2.1 The CV-ToF-ACSM

In this research, two CV-ToF-ACSM instruments (Aerodyne Research Inc., Billerica, MA) were deployed. One of the
instruments was located at a coastal site and one at an inland site to measure ambient aerosol composition. Both
instruments were operated with a 10-minute time resolution during ambient measurements. One of the instruments
was temporarily relocated to the laboratory for a calibration experiment (detailed in section 2.3), where it measured
110 with a 2-minute time resolution, and it was used in the AIDA chamber experiments (detailed in section 2.2), measuring
with a 5-minute time resolution.



Both CV-ToF-ACSM instruments were equipped with PM_{2.5} aerodynamic lens (Xu et al., 2017), which has proven to be very effective in detecting NR-PM_{2.5} with very good agreement against offline filter measurements (Liu et al., 2024). The CV-ToF-ACSM underwent regular calibrations as per established procedures (Canagaratna et al., 2007; 115 Fröhlich et al., 2013). These calibrations included flow rate, heater bias (HB) voltage, as well as calibrations for IE and relative ionization efficiency (RIE) for standard species (sulfate, nitrate, and ammonium). Data analysis was conducted using Tofware software (v3.2.4, Tofwerk AG, Thun, Switzerland) within the Igor Pro 8 environment.

2.2 AIDA Chamber experiments

120 The AIDA chamber is an experimental facility to study multi-phase chemical and physical processes under different atmospheric conditions, located in Karlsruhe, Germany (Bunz et al., 1996). The chamber has a volume of 84.5 m³ and a surface area of 103 m². In January 2024, a chamber simulation campaign was conducted as part of the CAINA project to simulate secondary organic aerosol formation pathways under various relative humidity (RH) conditions. Two experiments where NaCl aerosol was injected as a seed using an ultrasonic nebulizer with 0.1% aqueous solutions 125 were selected for this research. During both experiments, a temperature of 10°C was maintained. During the experiment of 18 January, a RH of between 0% and 1% was maintained, and during the experiment of 19 January the RH was between 90% and 95%. After injection of NaCl, SOA was produced by α -pinene ozonolysis, followed by the injection of NH₃ and NO₂, resulting in a complex organic aerosol (OA) mixing with the NaCl particles. During the experiments a TOF-ACSM measured the chemical composition of the aerosols in the reaction chamber. 130 Both experiments were performed over a duration of 8 – 9 hours.

2.3 Calibration experiment

Calibration of the ACSM with NaCl aerosol of various particles sizes was performed using the typical ACSM calibration setup as described by (Ng et al., 2011). NaCl aerosol was generated by nebulizing a 5 mMol L⁻¹ aqueous 135 solution with a Constant Output Atomizer (Model 3076, TSI Inc., Shoreview, MN, USA). The generated aerosol was directed through a silica gel diffusion dryer tube (Topas GmbH, DDU570 series) after which the aerosol reached a desired relative humidity of <40%. Monodisperse particles were generated by using the Vienna medium type differential mobility analyzer of the scanning mobility particle sizer (TROPOS-type SMPS). This SMPS is equipped with a butanol-based condensation particle counter (CPC) developed by TSI Instruments (model 3750, TSI Inc., 140 Shoreview, MN, USA). After the DMA, the desired aerosol concentration was adjusted using a diluter with a mixing tube provided by Aerodyne for the calibration of the ACSM. A butanol-based condensation particle counter (CPC) (model 3750, TSI Inc., Shoreview, MN, USA) was connected to the sampling pump connector of the ToF-ACSM to record the particle concentration at each selected size.

Measurements were performed with different concentrations and particle diameters of the NaCl aerosol. Three 145 different particle mobility diameters (150 nm, 200 nm and 250 nm) were selected for this research. For each particle diameter, the measurements were performed with three different aerosol concentrations ranging from 4.6 $\mu\text{g m}^{-3}$ – 26.3 $\mu\text{g m}^{-3}$. The duration of each measurement was ~15 minutes. However, only the data collected after the ACSM signal had stabilized were used for analysis (see fig. S1).



150 **2.4 Instrumental setup at the ambient measurement locations**

The first CV-ToF-ACSM is located at the Lutjewad coastal station, right next to the Wadden Sea dike at the Northern coast of the Netherlands at 53.24° N, 6.21° E. During Northerly wind directions, clean marine background air can reach the site. The direct surroundings of the measurement site can be considered rural and mainly consist of flat, agricultural land. Some small villages are located ±1 km southwest to southeast of the station. The nearest city is the

155 city of Groningen, which is located 23 km south- southwest of Lutjewad.

Ambient air was sampled at a flow rate of 40 L min⁻¹ through a 20-meter vertical stainless-steel inlet equipped with a PM_{2.5} size-selective impactor at the inlet head. At two meters height, a subsample of the flow is collected from the middle of the inlet at nearly isokinetic conditions and drawn into the sample container. Upon entry into the sampling container, the air stream was dried using a 300 mm Nafion membrane dryer (TROPOS). The dried air was

160 subsequently distributed to multiple instruments, including the CV-ToF-ACSM using a splitter developed by TROPOS (design 2019), featuring six ¼ inch outlet tubes and one ½ inch outlet tube, with a total flow rate of 16.7 L min⁻¹.

A second CV-ToF-ACSM is located 51.97° N, 4.93° E, in the Cabauw Experimental Site for Atmospheric Research (CESAR) tower. The location is managed and operated by the Royal Netherlands Meteorological Institute (KNMI).

165 The CESAR tower is located in the province of Utrecht, the Netherlands, approximately 45 km southeast of the North Sea coast. The site is located 45 km south of the city of Amsterdam, 31 km east of the city and port of Rotterdam, and 18 km southwest of the city of Utrecht. The direct surroundings of the CESAR tower can be considered rural and consist mainly of agricultural land and peat land. Although the site is not situated in a direct coastal environment, marine influences can still be observed under certain wind directions.

170 At the CESAR tower, ambient air was sampled for the CV-ToF-ACSM using a stainless-steel inlet system equipped with a PM_{2.5} size-cut cyclone (URG-2000-30ED) and a Nafion dryer. The sampling was conducted at a height of 4.5 m with a flow rate of 2 L min⁻¹.

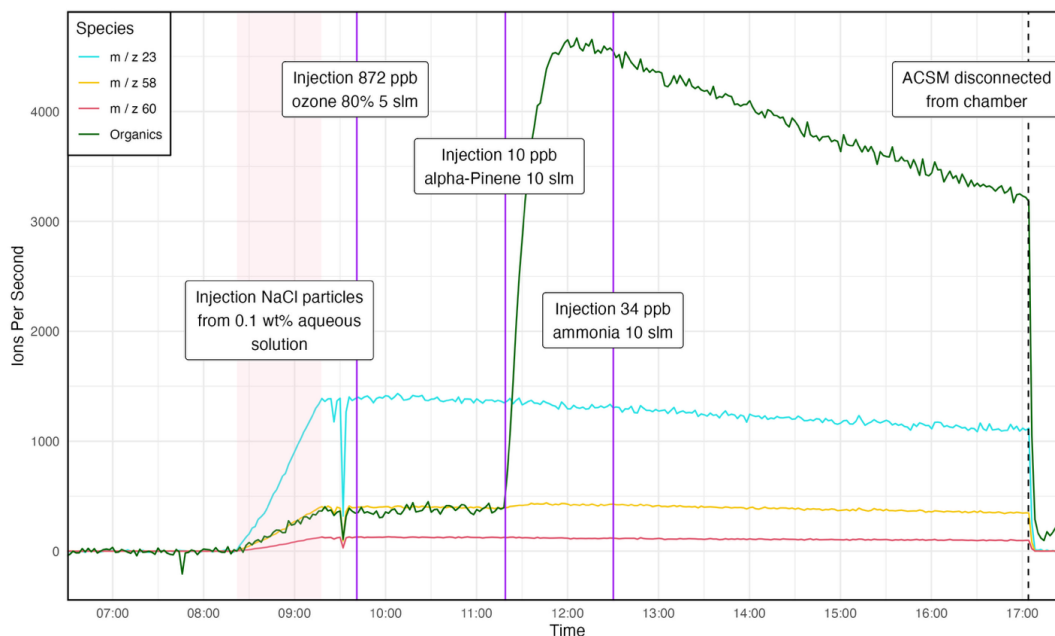
Meteorological data were retrieved from the Integrated Carbon Observation System (ICOS) and were recorded at a height of 60m for the Lutjewad measurement station. Hourly meteorological data for the CESAR tower site were

175 obtained from the KNMI database, measured at 10 m above ground level.

The datasets that were used cover the months January – August 2023, during which period both CV-ToF-ACSM instruments were measuring almost continuously. MeteoInfo software which makes use of the HYSPLIT model (Rolph et al., 2017; Stein et al., 2015) was used to retrieve the 72 hour air back-trajectories at both measurement sites.

180 **3 Results**

3.1 AIDA chamber data analysis



185 **Figure 1:** Time series of the fragment signals at m/z 23, m/z 58, and m/z 60 (light blue, yellow, and red, respectively), and
the organics signal as assigned by default in the fragmentation table of the TOF-ACSM, during the AIDA chamber
experiment on 18 January 2024. The pink shaded area represents the injection of NaCl particles from a 0.1 mass percent
190 (wt%) aqueous solution. The polydisperse aerosol had an average number mode diameter of ± 222 nm as derived from the
measurements with the two SMPS instruments. The purple shaded area and purple lines represent the injection of 872 ppb
ozone, the injection of 10 ppb α -pinene, and the injection of 34 ppb ammonia, respectively. α -pinene and ammonia
were injected with 10 standard liters per minute (slm). The black dashed line represents the time at which the ACSM
was disconnected from the chamber, resulting in all signals going to zero.

Figure 1 presents the time series of the aforementioned fragments, and the OA signal calculated using the default
fragmentation table for the ToF-ACSM during the AIDA chamber experiment conducted on 18 January 2024.
Injection of NaCl particles into the chamber results in rising signals for the fragments at m/z 23 (Na), m/z 58 (Na^{35}Cl)
195 and m/z 60 (Na^{37}Cl). The concurrent rise of the organic mass concentration is attributed to the fact that m/z 58 and
 m/z 60 are classified as OA fragments in the standard fragmentation table. The fragment at m/z 58 is the most dominant
contributor to the total OA signal in this experiment.

None of the three m/z signals under study were affected by the injection of ozone to the chamber environment.
Injection of 10 ppb α -Pinene resulted in a 10% increase of the signal at m/z 58 when considering the ions/s 3 minutes
200 prior to injection and 20 minutes after injection, and left the signals at m/z 23 and m/z 60 unaffected. These results
indicate that typical SOA does not seem to interfere significantly with the m/z signals at which NaCl is detected. Also,
the fragments at m/z 23, m/z 58 and m/z 60 were all found to have sufficiently high signals to serve as markers for the
presence of NaCl aerosol.

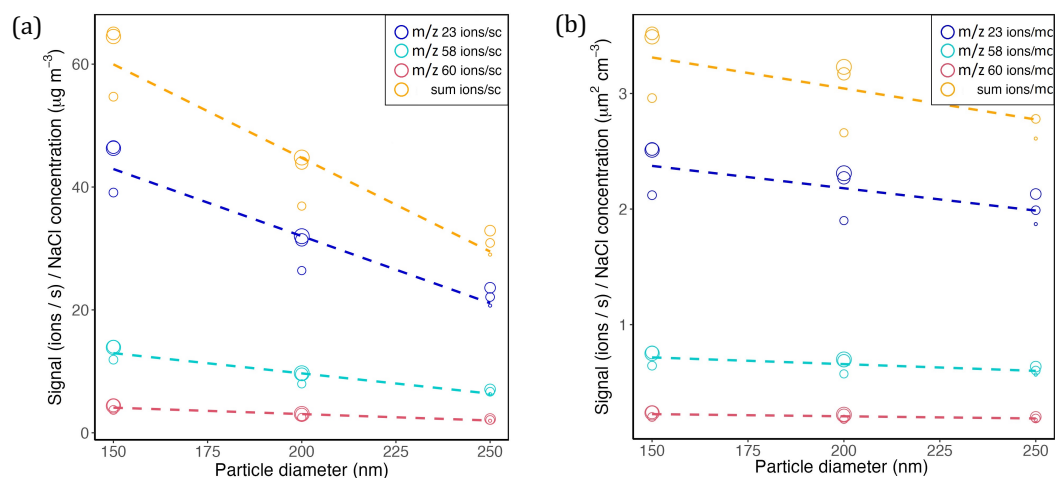
The experiment depicted in Fig. 1 was carried out under low relative humidity conditions (0 – 1% RH). A similar
205 experiment was conducted on 19 January 2024 under high relative humidity conditions (90 – 95% RH). Details of this
experiment are presented in fig. S2. As in the experiment on 18 January, the signals at m/z 23, m/z 58, and m/z 60



were not strongly affected by the addition of any of the injected chemicals. This further supports the conclusion that NaCl detection via these marker ions is robust against variations in humidity and the associated chemical and physical processes that occur under different RH conditions.

210

3.2 Quantification of NaCl using the CV-ToF-ACSM



215

Figure 2: Fragment signals normalized to NaCl mass (a) and surface concentration (b) at m/z 23, m/z 58, and m/z 60 as a function of different aerosol concentrations and particle sizes. The size of the markers is proportional to the NaCl aerosol concentration ranging from $4.6 \mu\text{g m}^{-3}$ to $26.3 \mu\text{g m}^{-3}$. The dark blue, light blue, red and orange markers respectively indicate the sum of the normalized signals at m/z 23, 58, 60 and the sum of these three signals (ions/s).

220

Figure 2a presents the ACSM signal normalized by the NaCl mass concentration as a function of particle mobility diameter. A systematic decrease in the normalized signal response with increasing particle size is observed. For NaCl aerosol particles with a diameter of 150 nm, the normalized signal is approximately a factor of two higher than that for particles with a diameter of 250 nm. The derived slopes (-0.22 , -0.066 , -0.021 , and -0.31 for m/z 23, m/z 58, m/z 60, and the summed NaCl fragments, respectively) indicate a consistent size-dependent decrease in signal response. This trend is consistently observed across all NaCl marker fragments, suggesting a uniform reduction in ACSM response with increasing particle size. In addition to particle size, the results suggest a slight, not entirely consistent aerosol concentration dependence. Lower concentrations generally yield marginally reduced signal responses for a given particle size and fragment ion. Notably, at NaCl concentrations below $\pm 10 \mu\text{g m}^{-3}$ the signal response decreases more strongly than for higher NaCl concentrations, reflecting reduced signal-to-noise ratios near the detection limit. Due to the observed size dependence, it is not possible to derive ambient sea salt mass concentrations from the ACSM signal without prior information on particle size.

225

230

To further investigate the observed size dependence, the ACSM signal was normalized by the total particle surface area concentration ($\mu\text{m}^2 \text{cm}^{-3}$) instead of mass (Fig. 2b). As shown in Fig. 2b, the normalized signal remains nearly constant across the full range of particle diameters, indicating that the ACSM response scales more closely with particle surface area than with aerosol mass. Linear regression analysis yields slopes close to zero for all NaCl marker fragments (-3.9×10^{-3} , -1.2×10^{-3} , and -3.8×10^{-4} for m/z 23, 58, and 60, respectively) as well as for the summed

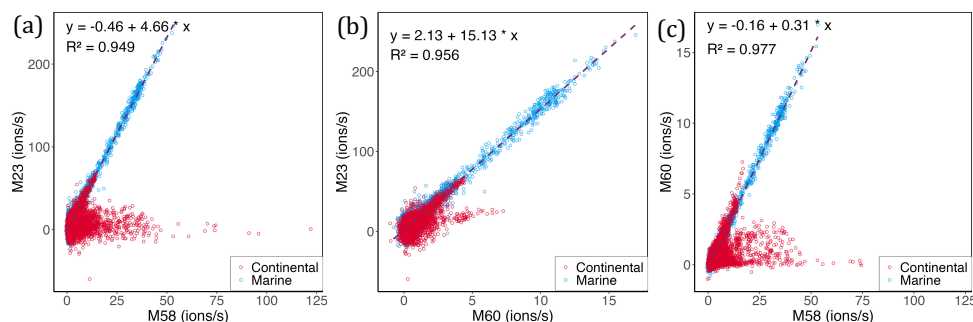


235 NaCl signal (-5.4×10^{-3}), confirming the absence of a strong size dependence when normalized by surface area. This
behavior likely arises from incomplete evaporation of NaCl in the CV, which operates as a surface-limited process
since only the particle surface area is in direct contact with the vaporizer. Particles with higher surface-to-volume
ratios therefore exhibit greater relative evaporation and correspondingly stronger signals. Normalizing by total surface
area thus enables the estimation of particle surface concentrations without requiring assumptions about particle size.

240

3.3 Ambient measurements

From January to August 2024, ambient aerosol composition was measured using the CV-ToF-ACSM at the Lutjewad
coastal station with a 10-minute time resolution. The measurement data was divided into two categories: marine air
(data recorded with wind angles between 280° and 70°) and continental air (data recorded with wind angles between
245 110° and 240°). The wind angle of the recorded data was based on hourly local wind measurements and the mismatch
between the ACSM data time resolution and the wind measurement time resolution was handled by matching the
ACSM measurements to the nearest recording of wind measurements. Furthermore the 72-hour air back trajectories
were investigated, and data assigned to marine air was discarded if the air back trajectory data indicated the air having
traveled over land mass of the mainland of The Netherlands or Germany to only investigate truly marine air (the use
250 of data of air having traveled over the Wadden Islands cannot be avoided, due to the placement of the islands relative
to the measurement location).

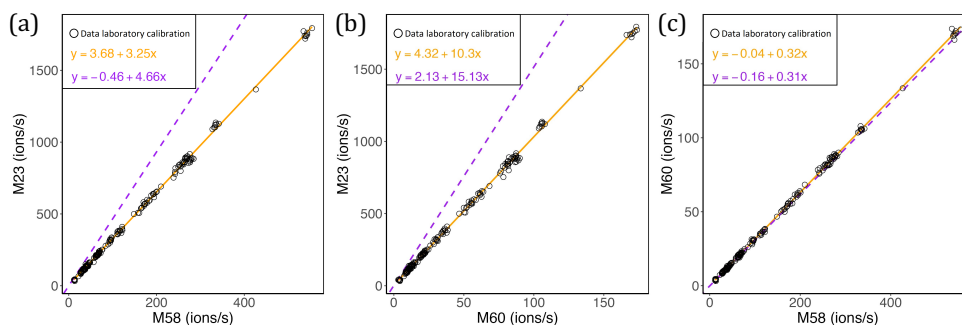


255 **Figure 3: Correlations between the signals of m/z 58 and m/z 23 (a), m/z 60 and m/z 23 (b), and m/z 58 and m/z 60 (c) in ions/s as measured at the Lutjewad measurement station. The dashed lines indicate the regression lines for the marine air data points.**

Figure 3 presents correlations between the ACSM signals of m/z 58 and m/z 60, m/z 58 and m/z 23, and m/z 60 and
m/z 23, respectively. A clear dependence on air mass origin is observed. Under marine-influenced conditions (onshore
260 wind), absolute signal intensities are significantly higher than under continental influence (offshore wind).
Furthermore, for marine air masses, the signal ratios remain highly consistent, with R^2 ranging from 0.946 to 0.951.
In contrast, no such correlation is observed for air masses originating from land, suggesting that the dominant source
of fragments of M58, M60 and M23 are sea salt when the air sample has traveled over sea. For continental air, some
of the measurements also indicate characteristic ratios of the fragments of M23, M58 and M60 associated with the
265 presence of sea salt. This could be explained by the fact that the Lutjewad measurement station is located directly at
the dike, and some sea salt aerosol can be present at the site, even with wind directions from land. The signal of m/z



270 23 shows scatter around 0, indicating that the measurement accuracy is lower at low aerosol concentrations than at high aerosol concentrations due to a relatively high limit of detection (LOD) for this fragment signal. This high LOD is likely influenced by an elevated instrumental background, which may be associated with vaporizer surface interactions and memory effects of semi-refractory sodium-containing species. Finally, the behavior of the signals at m/z 58 and m/z 60 suggests a source distinct from NaCl for continental air masses. While m/z 23 exhibits a stable signal ratio, m/z 58 shows increasing intensity independently of the other NaCl-related fragments during continental wind directions. This indicates that m/z 58 may be influenced by organic aerosol components or sources unrelated to sea salt. The m/z 60 signal also shows a distinct source during on-shore wind directions. The m/z 60 fragment is commonly used as a tracer for biomass burning aerosol in AMS and ACSM measurements (Alfarra et al., 2007; Schneider et al., 2006), originating mainly from levoglucosan ($C_6H_{10}O_5$), which is a pyrolysis product of cellulose formed during biomass combustion.



280 **Figure 4: Correlations between the signals of m/z 58 and m/z 23 (a), m/z 60 and m/z 23 (b), and m/z 58 and m/z 60 (c) in ions/s as measured during the calibration experiment (black markers). The orange solid lines represent the regression for the measured data during the calibration experiment. The dashed purple lines represent the regression for the measured ambient data at the Lutjewad measurement station, under marine airmass influences.**

285 Figure 4 shows the correlations between the ACSM signals at m/z 58 and m/z 60, m/z 58 and m/z 23, and m/z 60 and m/z 23 obtained during the calibration experiment as black points, and the corresponding regression line from the ambient samples in purple. As expected, relative intensities of m/z 23, m/z 58, and m/z 60 are highly correlated during the calibration experiment, confirming that all three signals originate from NaCl fragmentation. The slope of roughly 0.3 between m/z 60 and m/z 58 (Fig. 4c) corresponds well to the natural concentration ratios of the isotopologues, as the natural abundances of the ^{35}Cl and the ^{37}Cl isotopes (75.78% and 24.22%, respectively) result in an expected NaCl fragment ratio of 3.13. The ratios of m/z 58 and m/z 60 are nearly identical between calibration and ambient measurements (Fig. 4c), supporting the interpretation that a high correlation between these fragments reliably identifies NaCl in ambient data. In contrast, Figures 4a and 4b show a higher slope of the ambient measurements compared to the laboratory measurements, indicating that the relative intensity of m/z 23 is higher in the marine samples. This reduction in NaCl compared to the Na fragment points to chloride depletion, a characteristic feature of sea-salt ageing. During atmospheric processing, chloride in NaCl particles is displaced by acidic species such as HNO_3



or H_2SO_4 , resulting in partial replacement of Cl^- by nitrate or sulfate. The deviation of the slope from the nominal value can be used to assess the extent of chloride depletion as a characteristic feature of sea salt aging.

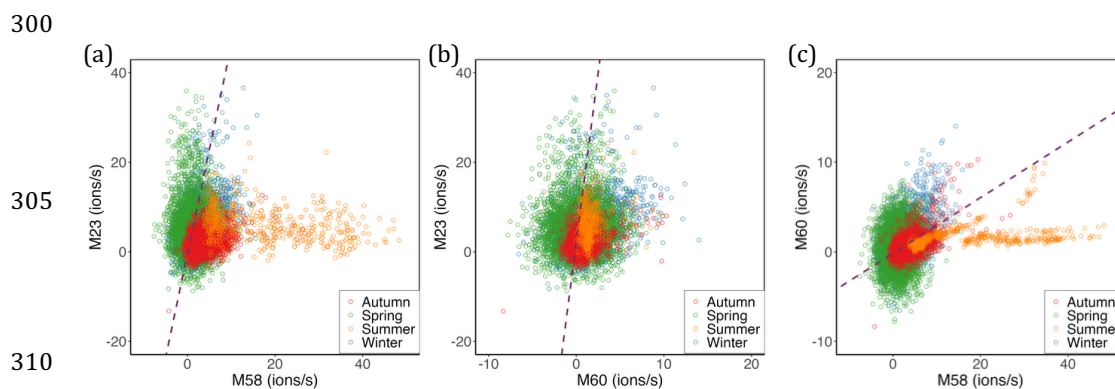


Figure 5: Correlations between the signals of m/z 58 and m/z 23 (a), m/z 60 and m/z 23 (b), and m/z 58 and m/z 60 (c) in ions/s, measured at the CESAR measurement site for continental air masses (defined as local wind directions between 22.5° and 157.5°). Dashed lines represent regression lines derived from marine air masses (as shown in Figure 3), highlighting typical fragment ratios observed for marine conditions. Summer months are defined as July, August and September, autumn months are defined as October, November, and December, winter months are defined as January, February and March, and spring months are defined as April, and May.

In order to test interferences at m/z of the NaCl signals by organic fragments, we analyzed a situation where NaCl is not expected. Figure 5 presents the correlations between the three ACSM marker ion signals (m/z 23, m/z 58 and m/z 60) measured at the CESAR site from May 2021 to April 2022, excluding June 2021 due to instrument downtime. Only data recorded with local wind directions between $22.5^\circ - 157.5^\circ$ are included, representing strictly continental air masses.

The fragment signals in ions/s for continental conditions show a similar range to those observed for a coastal site (Fig. 3) for m/z 58 and m/z 60. Specifically, m/z 58 generally spans from -10 to 50 ions/s, with most values between -10 and 10 ions/s. Similarly, m/z 60 ranges from -10 to 15 ions/s. However, Fig. 5c shows that m/z 58 and m/z 60 are not correlated with the characteristic slope of 0.3 showing that the increase in these fragments is not due to NaCl. The fragment signal of m/z 58 reaches much higher values in summer than in other seasons, indicating a source of this fragment which is only present in the summer months and unrelated to the fragment signals at m/z 23 and m/z 60. Therefore, the ratio between m/z 58 and m/z 60 serves as a reliable indicator to identify the presence of NaCl. In contrast, m/z 23 exhibits substantially lower intensities under continental air mass conditions, ranging from -10 to 35 ions/s, compared to the much higher values observed for marine air masses at the coastal site, which range from -15 to 220 ions/s (Fig. 3). This implies that there are continental sources of organic fragments at m/z 58 and m/z 60, which could interfere with the NaCl signal, if the air mass that is analysed is not strictly marine. Since m/z 23 is not affected by interfering masses and has the highest signal, it can be most reliably used to quantify the sea salt surface area concentrations. However, it is also the noisiest of all the signals, preventing quantification at very low concentrations. Based on the laboratory calibration described in Section 3.2, a linear relationship was derived between the signal $I_{m/z23}$ in ions/s at m/z 23 and the NaCl particle surface area concentration S_{NaCl} in $\mu\text{m}^2 \text{cm}^{-3}$. The NaCl surface area concentration can be calculated from the signal at m/z 23 as follows:



340

$$S_{NaCl} = 0.3808 * I_{m/z23} + 27.61 \quad (1)$$

The corresponding sensitivity is $0.381 \mu\text{m}^2 \text{cm}^{-3}$ per ions/s, with an R^2 of 0.995. As the background signal at m/z 23 is instrument specific, it must be determined individually for each CV-ToF-ACSM prior to application of this method. Equation 1. is also strictly only applicable to above-background m/z 23 signals. Using this relationship for marine air masses at the coastal site, we show significant concentrations of NaCl up to $121 \mu\text{m}^2 \text{cm}^{-3}$. These concentrations correspond to NaCl before ageing.

345

4 Conclusions

The addition of the CV to the ACSM significantly reduces particle bounce effects, thereby decreasing measurement uncertainties. An additional consequence of using a CV is that some refractory particles, such as sea salt can also be detected by using instruments equipped with a CV system due to the prolonged time the particles spend in the vaporizer. This study demonstrates that the CV-ToF-ACSM can effectively detect sodium chloride (NaCl), using distinct mass fragments at m/z 23 (Na^+), m/z 58 (Na^{35}Cl), and m/z 60 (Na^{37}Cl) as reliable markers. These fragments exhibit high signal strengths and minimal interference from a range of organic fragments and complex chemical processing in the atmosphere. Laboratory experiments revealed that the ACSM response to NaCl aerosol is more closely related to available particle surface area than to total aerosol mass. A slight concentration dependence of the ACSM signal normalized to aerosol surface concentration was observed, with lower aerosol concentrations resulting in proportionally weaker signals. Field measurements at a coastal site confirmed strong positive correlations between the fragment signals at m/z 23, m/z 58 and m/z 60 when sampling marine air. In continental air, masses interferences from organic fragments at m/z 58 and m/z 60 are present, but can be distinguished by a missing correlation between m/z 58 and m/z 60. Based on the laboratory experiments, a quantitative relationship between the m/z 23 signal and NaCl particle surface concentrations was established and subsequently used to derive a method for quantifying atmospheric NaCl prior to chemical ageing. This approach enables the calculation of NaCl surface area concentrations directly from the CV-ToF-ACSM m/z 23 signal using a calibration-based formula, allowing for the identification and quantification of freshly emitted sea-salt aerosol. These findings highlight the CV-ToF-ACSM as an effective tool for quantifying and monitoring sea-salt aerosol abundance and processing in the atmosphere, providing a solid foundation for studies of chemical ageing and particle composition on marine environments.

350

355

360

365

370 Data availability

All raw data can be provided by the corresponding authors upon request.

Author contributions

JM, UD and MvdB performed the ambient measurements. MvdB and UD analyzed the ambient data. HS, JF, HJO, JM and UD performed the AIDA chamber experiments. HJO, JF, and MvdB analyzed the AIDA chamber data. MvdB and JM performed the laboratory experiments. MvdB and UD analyzed the laboratory data. MvdB wrote the manuscript. HJO, JM, JF, HS and UD reviewed and edited the manuscript.

375



Competing interests

The authors declare that they have no conflict of interest.

380

Acknowledgements

This work was carried out using data from the Ruisdael Observatory as part of its continuous monitoring efforts. The authors gratefully acknowledge Davide Merlo for his valuable assistance with the laboratory experiments.

385 Financial support

This research has been supported by the Cloud-Aerosol Interactions in a Nitrogen-dominated Atmosphere (CAINA) project (grant no. OCENW.XL21.XL21.112) and the ATMO-ACCESS project (ATMO-TNA-3 – 0000000063). The Ruisdael Observatory is a scientific infrastructure co-financed by the Dutch Research Council (NWO, 184.034.015).

390 References

- Alfarra, M. R., Prevot, A. S. H., Szidat, S., Sandradewi, J., Weimer, S., Lanz, V. A., Schreiber, D., Mohr, M., and Baltensperger, U.: Identification of the Mass Spectral Signature of Organic Aerosols from Wood Burning Emissions, *Environ. Sci. Technol.*, 41, 5770–5777, <https://doi.org/10.1021/es062289b>, 2007.
- 395 Bahreini, R., Jimenez, J. L., Wang, J., Flagan, R. C., Seinfeld, J. H., Jayne, J. T., and Worsnop, D. R.: Aircraft-based aerosol size and composition measurements during ACE-Asia using an Aerodyne aerosol mass spectrometer, *J. Geophys. Res. Atmospheres*, 108, <https://doi.org/10.1029/2002JD003226>, 2003.
- Bates, T. S., Quinn, P. K., Frossard, A. A., Russell, L. M., Hakala, J., Petäjä, T., Kulmala, M., Covert, D. S., Cappa, C. D., Li, S.-M., Hayden, K. L., Nuaaman, I., McLaren, R., Massoli, P., Canagaratna, M. R., Onasch, T. B., Sueper, D., Worsnop, D. R., and Keene, W. C.: Measurements of ocean derived aerosol off the coast of California, *J. Geophys. Res. Atmospheres*, 117, <https://doi.org/10.1029/2012JD017588>, 2012.
- 400 Bellouin, N., Quaas, J., Gryspeerdt, E., Kinne, S., Stier, P., Watson-Parris, D., Boucher, O., Carslaw, K. S., Christensen, M., Daniau, A. -L., Dufresne, J. -L., Feingold, G., Fiedler, S., Forster, P., Gettelman, A., Haywood, J. M., Lohmann, U., Malavelle, F., Mauritsen, T., McCoy, D. T., Myhre, G., Mülmenstädt, J., Neubauer, D., Possner, A., Rugenstein, M., Sato, Y., Schulz, M., Schwartz, S. E., Sourdeval, O., Storelvmo, T., Toll, V., Winker, D., and Stevens, B.: Bounding Global Aerosol Radiative Forcing of Climate Change, *Rev. Geophys. Wash. DC* 1985, 58, e2019RG000660, <https://doi.org/10.1029/2019RG000660>, 2020.
- Bunz, H., Möhler, O., Naumann, K.-H., Saathoff, H., Schöck, W., and Schurath, U.: The novel aerosol chamber facility AIDA: status and first results, 1996.
- 410 Canagaratna, M. R., Jayne, J. T., Jimenez, J. L., Allan, J. D., Alfarra, M. R., Zhang, Q., Onasch, T. B., Drewnick, F., Coe, H., Middlebrook, A., Delia, A., Williams, L. R., Trimborn, A. M., Northway, M. J., DeCarlo, P. F., Kolb, C. E., Davidovits, P., and Worsnop, D. R.: Chemical and microphysical characterization of ambient aerosols with the aerodyne aerosol mass spectrometer, *Mass Spectrom. Rev.*, 26, 185–222, <https://doi.org/10.1002/mas.20115>, 2007.
- 415 Freney, E., Sellegri, K., Nicosia, A., Williams, L. R., Rinaldi, M., Trueblood, J. T., Prévôt, A. S. H., Thyssen, M., Grégori, G., Haëntjens, N., Dinasquet, J., Obernosterer, I., Van Wambeke, F., Engel, A., Zäncker, B., Desboeufs, K., Asmi, E., Timonen, H., and Guieu, C.: Mediterranean nascent sea spray organic aerosol and relationships with seawater biogeochemistry, *Atmospheric Chem. Phys.*, 21, 10625–10641, <https://doi.org/10.5194/acp-21-10625-2021>, 2021.
- Fröhlich, R., Cubison, M. J., Slowik, J. G., Bukowiecki, N., Prévôt, A. S. H., Baltensperger, U., Schneider, J., Kimmel, J. R., Gonin, M., Rohner, U., Worsnop, D. R., and Jayne, J. T.: The ToF-ACSM: a portable aerosol chemical speciation



- 420 monitor with TOFMS detection, *Atmospheric Meas. Tech.*, 6, 3225–3241, <https://doi.org/10.5194/amt-6-3225-2013>, 2013.
- Lee, L. A., Reddington, C. L., and Carslaw, K. S.: On the relationship between aerosol model uncertainty and radiative forcing uncertainty, *Proc. Natl. Acad. Sci.*, 113, 5820–5827, <https://doi.org/10.1073/pnas.1507050113>, 2016.
- 425 Liu, X., Henzing, B., Hensen, A., Mulder, J., Yao, P., van Dinter, D., van Bronckhorst, J., Huang, R., and Dusek, U.: Measurement report: Evaluation of the TOF-ACSM-CV for PM_{1.0} and PM_{2.5} measurements during the RITA-2021 field campaign, *Atmospheric Chem. Phys.*, 24, 3405–3420, <https://doi.org/10.5194/acp-24-3405-2024>, 2024.
- Mallet, M., Cravigan, L., Miljevic, B., Vaattovaara, P., Deschaseaux, E., Swan, H., Jones, G., and Ristovski, Z.: Sea spray aerosol in the Great Barrier Reef and the presence of nonvolatile organics, *J. Geophys. Res. Atmospheres*, 121, 7088–7099, <https://doi.org/10.1002/2016JD024966>, 2016.
- 430 Ng, N. L., Herndon, S. C., Trimborn, A., Canagaratna, M. R., Croteau, P. L., Onasch, T. B., Sueper, D., Worsnop, D. R., Zhang, Q., Sun, Y. L., and Jayne, J. T.: An Aerosol Chemical Speciation Monitor (ACSM) for Routine Monitoring of the Composition and Mass Concentrations of Ambient Aerosol, *Aerosol Sci. Technol.*, 45, 780–794, <https://doi.org/10.1080/02786826.2011.560211>, 2011.
- 435 Nuaaman, I., Li, S.-M., Hayden, K. L., Onasch, T. B., Massoli, P., Sueper, D., Worsnop, D. R., Bates, T. S., Quinn, P. K., and McLaren, R.: Separating refractory and non-refractory particulate chloride and estimating chloride depletion by aerosol mass spectrometry in a marine environment, <https://doi.org/10.5194/acpd-15-2085-2015>, 22 January 2015.
- O’Dowd, C. D. and Smith, M. H.: Physicochemical properties of aerosols over the northeast Atlantic: Evidence for wind-speed-related submicron sea-salt aerosol production, *J. Geophys. Res. Atmospheres*, 98, 1137–1149, <https://doi.org/10.1029/92JD02302>, 1993.
- 440 O’Dowd, C. D., Jimenez, J. L., Bahreini, R., Flagan, R. C., Seinfeld, J. H., Hämeri, K., Pirjola, L., Kulmala, M., Jennings, S. G., and Hoffmann, T.: Marine aerosol formation from biogenic iodine emissions, *Nature*, 417, 632–636, <https://doi.org/10.1038/nature00775>, 2002.
- 445 Ovadnevaite, J., Ceburnis, D., Canagaratna, M., Berresheim, H., Bialek, J., Martucci, G., Worsnop, D. R., and O’Dowd, C.: On the effect of wind speed on submicron sea salt mass concentrations and source fluxes, *J. Geophys. Res. Atmospheres*, 117, <https://doi.org/10.1029/2011JD017379>, 2012.
- Petters, S. S., Kjærgaard, E. R., Hasager, F., Massling, A., Glasius, M., and Bilde, M.: Morphology and hygroscopicity of nanoplastics in sea spray, *Phys. Chem. Chem. Phys.*, 25, 32430–32442, <https://doi.org/10.1039/D3CP03793B>, 2023.
- 450 Rolph, G., Stein, A., and Stunder, B.: Real-time Environmental Applications and Display sYstem: READY, *Environ. Model. Softw.*, 95, 210–228, <https://doi.org/10.1016/j.envsoft.2017.06.025>, 2017.
- Saathoff, H., Naumann, K.-H., Möhler, O., Jonsson, Å. M., Hallquist, M., Kiendler-Scharr, A., Mentel, T. F., Tillmann, R., and Schurath, U.: Temperature dependence of yields of secondary organic aerosols from the ozonolysis of α -pinene and limonene, *Atmospheric Chem. Phys.*, 9, 1551–1577, <https://doi.org/10.5194/acp-9-1551-2009>, 2009.
- 455 Schmale, J., Schneider, J., Nemitz, E., Tang, Y. S., Dragosits, U., Blackall, T. D., Trathan, P. N., Phillips, G. J., Sutton, M., and Braban, C. F.: Sub-Antarctic marine aerosol: dominant contributions from biogenic sources, *Atmospheric Chem. Phys.*, 13, 8669–8694, <https://doi.org/10.5194/acp-13-8669-2013>, 2013.
- Schneider, J., Weimer, S., Drewnick, F., Borrmann, S., Helas, G., Gwaze, P., Schmid, O., Andreae, M. O., and Kirchner, U.: Mass spectrometric analysis and aerodynamic properties of various types of combustion-related aerosol particles, *Int. J. Mass Spectrom.*, 258, 37–49, <https://doi.org/10.1016/j.ijms.2006.07.008>, 2006.



- 460 Stein, A. F., Draxler, R. R., Rolph, G. D., Stunder, B. J. B., Cohen, M. D., and Ngan, F.: NOAA's HYSPLIT Atmospheric Transport and Dispersion Modeling System, *Bull. Am. Meteorol. Soc.*, 96, 2059–2077, <https://doi.org/10.1175/BAMS-D-14-00110.1>, 2015.
- 465 Sutresna, A., Keywood, M., Paton-Walsh, C., Simmons, J., Mynard, C., Dang, Q., Mochida, M., Ohata, S., Afsana, S., Kunwar, B., Kawamura, K., Humphries, R., Dunne, E., Ward, J., Harnwell, J., Reisen, F., Emmerson, K., Griffiths, A., Williams, A., Schofield, R., and Rayner, P.: Interference of sea salt in capture vaporizer-ToF-ACSM measurements of biomass burning organic aerosols in coastal locations, *Environ. Sci. Atmospheres*, 4, 634–644, <https://doi.org/10.1039/D3EA00171G>, 2024.
- 470 Timonen, H., Cubison, M., Aurela, M., Brus, D., Lihavainen, H., Hillamo, R., Canagaratna, M., Nekat, B., Weller, R., Worsnop, D., and Saarikoski, S.: Applications and limitations of constrained high-resolution peak fitting on low resolving power mass spectra from the ToF-ACSM, *Atmospheric Meas. Tech.*, 9, 3263–3281, <https://doi.org/10.5194/amt-9-3263-2016>, 2016.
- 475 Wagner, R., Ickes, L., Bertram, A. K., Els, N., Gorokhova, E., Möhler, O., Murray, B. J., Umo, N. S., and Salter, M. E.: Heterogeneous ice nucleation ability of aerosol particles generated from Arctic sea surface microlayer and surface seawater samples at cirrus temperatures, *Atmospheric Chem. Phys.*, 21, 13903–13930, <https://doi.org/10.5194/acp-21-13903-2021>, 2021.
- Xu, W., Croteau, P., Williams, L., Canagaratna, M., Onasch, T., Cross, E., Zhang, X., Robinson, W., Worsnop, D., and Jayne, J.: Laboratory characterization of an aerosol chemical speciation monitor with PM_{2.5} measurement capability, *Aerosol Sci. Technol.*, 51, 69–83, <https://doi.org/10.1080/02786826.2016.1241859>, 2017.
- 480 Xu, W., Lambe, A., Silva, P., Hu, W., Onasch, T., Williams, L., Croteau, P., Zhang, X., Renbaum-Wolff, L., Fortner, E., Jimenez, J. L., Jayne, J., Worsnop, D., and Canagaratna, M.: Laboratory evaluation of species-dependent relative ionization efficiencies in the Aerodyne Aerosol Mass Spectrometer, *Aerosol Sci. Technol.*, 52, 626–641, <https://doi.org/10.1080/02786826.2018.1439570>, 2018.
- 485 Zhang, Q., Jimenez, J. L., Canagaratna, M. R., Ulbrich, I. M., Ng, N. L., Worsnop, D. R., and Sun, Y.: Understanding atmospheric organic aerosols via factor analysis of aerosol mass spectrometry: a review, *Anal. Bioanal. Chem.*, 401, 3045–3067, <https://doi.org/10.1007/s00216-011-5355-y>, 2011.
- Zheng, Y., Cheng, X., Liao, K., Li, Y., Li, Y. J., Huang, R.-J., Hu, W., Liu, Y., Zhu, T., Chen, S., Zeng, L., Worsnop, D. R., and Chen, Q.: Characterization of anthropogenic organic aerosols by TOF-ACSM with the new capture vaporizer, *Atmospheric Meas. Tech.*, 13, 2457–2472, <https://doi.org/10.5194/amt-13-2457-2020>, 2020.
- 490 Zorn, S. R., Drewnick, F., Schott, M., Hoffmann, T., and Borrmann, S.: Characterization of the South Atlantic marine boundary layer aerosol using an aerodyne aerosol mass spectrometer, *Atmospheric Chem. Phys.*, 8, 4711–4728, <https://doi.org/10.5194/acp-8-4711-2008>, 2008.